Journal of Heat and Mass Transfer Research

Unsteady boundary layer flow of a Casson fluid past a wedge with wall slip velocity

Sarojamma Ganganapalli*, Sreelakshmi Kata and Vasundhara Bhumarapu

Sri Padmavati Mahila Visvavidyalayam, Tirupati, Andhra Pradesh, 517502, India

A B S T R A C T

In this paper, an analysis is presented to understand the effect of non-Newtonian rheology, velocity slip at boundaries, thermal radiation, heat absorption/generation, and first-order chemical reactions on unsteady MHD mixed convective heat and mass transfer of a Casson fluid past a wedge in the presence of a transverse magnetic field with variable electrical conductivity. The partial differential equations governing the flow with the pertinent boundary conditions were solved numerically. The computational results are presented graphically for different values of the non-dimensional parameters of the analysis. The results for particular cases were compared with the published results available in the literature and were found to be in excellent agreement. The present analysis indicates that the Casson parameter for representing non-Newtonian rheology has an increasing influence on velocity and temperature. The point of flow separation was found for negative values of the wedge angle parameter. The radiation parameter enhances the rate of heat transfer. The mass transfer rate is reduced with chemical reaction parameter and Schmidt's number.

1. Introduction

Fluids flowing over wedge-shaped bodies find abundant thermal engineering applications in crude oil extraction [1], geothermal systems [2], ground water pollution [3], heat exchangers, and the storage of nuclear waste [4], etc. The steady laminar boundary flow of a Newtonian fluid over a wedge was first studied by Falkner and Skan [5], and the governing equations of the problem are solved numerically by employing suitable similarity variables. The same problem was subsequently discussed by Hartree [6] in detail by considering different values of the wedge angle. Yih [7] investigated the Magnetohydrodynamic (MHD) forced convection flow over a wedge with viscous dissipation and variable wall temperature on the surface of the wedge. Their results show that the local skin friction coefficient and local Nusselt number increase with an increasing pressure gradient parameter and magnetic parameter. The decreasing Eckert number enhanced the local Nusselt number. Chamka [8] extended the Yih's study [7] by including the effects of suction or injection, temperature-dependent heat generation or absorption, and thermal radiation. It was noticed that wall suction tends to reduce the thickness of the hydrodynamic and thermal boundary layers. The local skin friction coefficient and Nusselt number were found to increase with increasing suction, and the increasing pressure gradient parameter reduced both velocity and temperature. The thermal radiation parameter increased conduction with a rise in temperature. Anjali Devi and Kandaswamy [9]

Corresponding Author : Sri Padmavati Mahila Visvavidyalayam, Tirupati, Andhra Pradesh, 517502, India
Email : gsarojamma@gmail.com

investigated the effects of heat and mass transfer on MHD laminar boundary layer flow over a wedge with suction or injection. They observed that the flow field is influenced appreciably by the magnetic field and suction or injection at the wall of the wedge. Kandaswamy et al. [10] discussed the effects of a chemical reaction on heat and mass transfer and the flow over a porous wedge with thermal radiation in the presence of suction/injection. Their numerical calculation reveals that the flow field is significantly influenced by chemical reactions, the buoyancy ratio between species and thermal diffusion, and suction/injection at wall surface. Singh et al. [4] studied unsteady mixed convection and mass transfer of a viscous, incompressible fluid over a vertical wedge with constant suction and injection. They observed that the buoyancy force increases the velocity considerably with an overshoot for low–Prandtl number fluids. Fluid drag, heat, and mass transfer rates were changed significantly due to injection/suction for both accelerating and decelerating flows. Ganapathirao et al. [11] studied the effects of non-uniform single and double slot suction (injection) on an unsteady, mixed convection boundary layer flow over a vertical wedge with a chemical reaction and heat generation or absorption. They observed that the skin friction, heat, and mass transfer coefficients increase with non-uniform slot suction, but the effect of non-uniform slot injection is just the opposite. As the slot moves in the downstream direction, the skin friction, heat, and mass transfer coefficient decreased in non-uniform slot suction, whereas non-uniform slot injection has the reverse effect. Ahmad and Khan [12] investigated the heat and mass transfer of a MHD viscous flow over a moving wedge, considering the effects of viscous dissipation, heat sources/sinks, and a convective boundary condition.

It is well known that the majority of fluids used in various technological and industrial applications are non-Newtonian. Each non-Newtonian fluid is described separately with its unique constitutive equation. Keimanesh et al. [13] examined the flow of a third-grade non-Newtonian fluid between two parallel plates using the effective multistep differential transform method. In all of the above studies, the fluid under investigation is Newtonian. The study of non-Newtonian fluid flows over a wedge has significant engineering applications. Rajagopal et al. [14] studied the Falknar–Skan flow of a homogenous, incompressible second-grade fluid past a wedge placed symmetrically to the flow direction. Hady and Hassanien [15] extended Rajagopal et al.'s study [14] by including the effects of magnetic fields and porosity. Rashidi et al. [16] explored the thermal characteristics of a generalized, third-grade, viscoelastic power-law fluid over a permeable wedge employing HAM. Alam and Hossain [17], using a new class of similarity transformation, obtained a local similarity solution to

the unsteady, two-dimensional forced convective heat transfer flow of a micropolar fluid along a wedge. Their results indicate that as the wedge angle parameter increases, the growth of the thickness of the hydrodynamic and thermal boundary layers decrease. The velocity was found to increase whereas both microrotation and temperature profiles were found to decrease with increasing values of the unsteadiness parameter. Rostami et al. [18] made a numerical investigation of laminar viscoelastic fluid flow over a wedge in the presence of a buoyancy force by considering an external varying velocity and observed that the local skin friction coefficient decreased with the Prandtl number in the case of assisting flow and a reversal behavior in the case of opposing flow. The viscoelastic parameter was observed to reduce the Nusselt number. The impact of the Prandtl number and wedge angle parameter was observed to decrease the thickness of boundary layer.

A Casson fluid is a non-Newtonian fluid that shows a dual behavior whose constitutive equation was described by Casson [19] while studying the flow profiles of printing inks. When the shear stress is less than the yield stress, a Casson fluid moves together as if it were a solid, and when the shear stress is greater than the yield stress, it behaves like a fluid. Casson fluid models have been used to describe industrial polymers [20] and silicon suspension [21]. Blood, being a suspension of cells in plasma, has a dual behavior as well, i.e., at higher shear rates it behaves as a Newtonian fluid, and at lower shear rates it has a highly non-Newtonian nature [22, 23]. A Casson fluid model described blood satisfactorily and accounted for the dual behavior [23].

Studies pertaining to flow past a wedge in Casson fluids are very limited. Swati et al. [24] made an investigation into the boundary layer flow of a Casson fluid over a symmetric wedge. They observed that with an increase in the Casson fluid parameter, the fluid velocity is increased while the temperature is reduced. In a subsequent paper, Swati and Mandal [25] extended the above problem with surface heat flux. Their results show that the fluid velocity is suppressed with an increase of suction, and flow separation is controlled by increasing values of the Casson parameter and suction parameter.

In all the foregoing studies, the flow field is assumed to obey the no-slip boundary condition. However, there are situations where the no-slip condition at the boundary does not hold and, hence, requires that it is replaced by the partial slip boundary condition. For instance, when the boundary surface is made of certain coated surfaces, a certain degree of tangential slip exists. It has also been reported that fluids with boundary slip find applications in technological problems like polishing artificial valves and internal cavities.

In this paper, we made an effort to investigate the effects of velocity slip at the surface, heat generation/ absorption, and thermal radiation in the presence of a chemical reaction on the heat and mass transfer flow of a Casson fluid past a wedge under the influence of a magnetic field. The flow is exposed to a uniform magnetic field in the direction of the flow. Employing suitable similarity transformations, the nonlinear partial differential equations describing the momentum, energy, and species concentration were converted into a set of coupled, nonlinear differential equations. This reduced set of equations together with the pertinent boundary conditions were solved numerically using the Runge-Kutta method along with the shooting technique. The parametric analysis of the flow variables was performed in detail for various sets of the governing parameters that emerge in the mathematical analysis.

2. Mathematical formulation

Consider the unsteady, laminar, two-dimensional transfer flow of an incompressible, electrically conductive Casson fluid along an impermeable wedge in the presence of non-uniform heat generation/absorption. The angle of the wedge is taken as $\Omega = \delta\pi$. The flow is assumed to be in the x direction, which is considered to be along a direction of the wedge, and the y axis is normal to it. A magnetic field $B(x,t)$ is applied in the positive y direction as shown in Fig. 1. The magnetic Reynolds number is assumed to be very small, and hence, the induced magnetic field is neglected. The effect of thermal radiation and a first-order chemical reaction is taken into account in the present analysis. The surface of the wedge is maintained at a constant temperature T_w, which is assumed to be higher than the ambient temperature T_∞. The concentration at the wedge surface takes the constant value C_w, while the ambient value attained as y tends to infinity takes the constant value C_∞.

The flow is governed by the rheological equation of the state of the Casson fluid that can be written as [26]

$$\tau_{ij} = \begin{cases} 2\left(\mu_B + \frac{\tau_y}{\sqrt{2\pi}}\right) e_{ij}, & \pi > \pi_c, \\ 2\left(\mu_B + \frac{\tau_y}{\sqrt{2\pi}}\right) e_{ij}, & \pi < \pi_c. \end{cases} \quad (1)$$

where μ_B is the plastic dynamic viscosity of the non-Newtonian fluid, τ_y is the yield stress of the fluid, π is the product of the component of the deformation rate with itself (namely, $\pi = e_{ij}e_{ij}$), e_{ij} is the (i, j)th component of the deformation rate, and π_c is the critical value of π based on the non-Newtonian model.
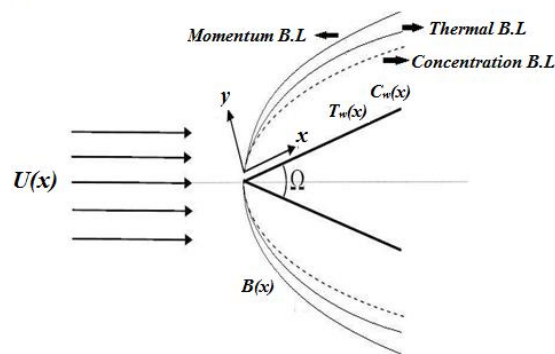

Fig. 1. Physical model and coordinate system

Making use of the Boussinesq and Rosseland approximations, the basic governing equations describing the conservation of mass, momentum, energy, and concentration, respectively, can be written as follows [12]:

$$\frac{\partial u}{\partial x} + \frac{\partial v}{\partial y} = 0, \quad (2)$$

$$\frac{\partial u}{\partial t} + u\frac{\partial u}{\partial x} + v\frac{\partial u}{\partial y} = \frac{\partial U}{\partial t} + U\frac{\partial U}{\partial x} + \left(1 + \frac{1}{\beta}\right)v\frac{\partial^2 u}{\partial y^2} - \frac{\sigma(B(x,t))^2}{\rho}(u - U), \quad (3)$$

$$\rho c_p\left(\frac{\partial T}{\partial t} + u\frac{\partial T}{\partial x} + v\frac{\partial T}{\partial y}\right) = k\frac{\partial^2 T}{\partial y^2} + \frac{16\sigma^* T_\infty^3}{3K^*}\frac{\partial^2 T}{\partial y^2} + q''', \quad (4)$$

$$\frac{\partial C}{\partial t} + u\frac{\partial C}{\partial x} + v\frac{\partial C}{\partial y} = D\frac{\partial^2 C}{\partial y^2} - k_1(C - C_\infty), \quad (5)$$

where u and v are velocity components in the x and y directions, respectively. The kinematic coefficient of viscosity is v; $\beta = \mu_B\sqrt{2\pi_c/\tau_y}$ is the parameter of the Casson fluid; σ is the electrical conductivity, which is assumed to have a variable property; T is the fluid temperature; C is the concentration; ρ is the density of the fluid; σ^* is the Stefen-Boltzman constant; K^* is the absorption coefficient; q''' is the coefficient of the rate of internal heat generation (> 0) or absorption (< 0); D is the mass diffusivity; c_p is the specific heat at constant pressure; k is the thermal conductivity; and k_1 is the chemical reaction. The internal heat generation or absorption term q''' is modeled according to the following equation [27]:

$$q''' = \left(\frac{\lambda_g U \Delta T}{x\vartheta}\right)[A^*(T_w - T_\infty)e^{-\eta} + B^*(T - T_\infty). \quad (6)$$

Here, A^* and B^* are the coefficients of space-dependent and temperature-dependent internal heat generation or absorption on the space coordinates. The case when both $A^* > 0$ and $B^* > 0$ corresponds to internal heat generation, while when both $A^* < 0$ and $B^* < 0$ corresponds to internal heat absorption.

For the unsteady flow state, it is appropriate to assume that the applied magnetic field strength

$B(x, t)$ is of the form $B(x, t) = B_0\sqrt{\delta_1/x}$, where B_0 is a constant, and the electrical conductivity has the form $\sigma = \sigma_0(u - U)$, where σ_0 is constant. Substituting $B(x, t)$ and σ in Equation (3), we get

$$\frac{\partial u}{\partial t} + u\frac{\partial u}{\partial x} + v\frac{\partial u}{\partial y} = \frac{\partial U}{\partial t} + U\frac{\partial U}{\partial x} + \left(1 + \frac{1}{\beta}\right)v\frac{\partial^2 u}{\partial y^2} - \frac{\sigma_0 B_0^2 \delta_1}{\rho x}(u - U)^2. \tag{7}$$

The boundary conditions are
$$u = L(\partial u/\partial y), v = 0 \; ; \; T = T_w, C = C_w \qquad \text{at} \\ y = 0 \\ u = U(x, t), \; T \to T_\infty, \; C \to C_\infty, \; as \; y \to \infty, \tag{8}$$

where $U(x, t) = \frac{vx^m}{\delta_1^{m+1}}$ is the potential flow velocity for the wedge flow, m is an arbitrary constant and is related to the wedge angle, and $\delta_1 = \delta_1(t)$ is the time-dependent length scale. We define the stream function $\Psi(x, y)$, satisfying the continuity Equation (1), as $u = \frac{\partial\Psi}{\partial y}$, $v = -\frac{\partial\Psi}{\partial x}$.

We introduce the following the similarity variables [28]:

$$\eta = y\sqrt{\frac{(1+m)}{2}}\sqrt{\frac{x^{m-1}}{\delta_1^{m+1}}}, \; \Psi = \sqrt{\frac{2}{m+1}}\sqrt{\frac{vx^{m+1}}{\delta_1^{m+1}}}f(\eta), \\ \theta = T - T_\infty/T_w - T_\infty, \phi = C - C_\infty/C_w - C_\infty. \tag{9}$$

On substituting Equation (9) in Equations (7), (4), and (5), they reduce to
$$\left(1 + \frac{1}{\beta}\right)f''' + ff'' + \delta(1 - f'^2) - \frac{\delta_1^m}{vx^{m-1}}\frac{d\delta_1}{dt}(2 - 2f' - \eta f'') - \frac{2}{(m+1)}M(f' - 1)^2 = 0, \tag{10}$$

$$\left(1 + \frac{4}{3}Nr\right)\theta'' + Pr\frac{\delta_1^m}{vx^{m-1}}\frac{d\delta_1}{dt}\eta\theta' + Prf\theta' + \frac{2}{m+1}[A^*e^{-\eta} + B^*\theta] = 0, \tag{11}$$

$$\phi'' + Scf\phi' + \frac{\delta_1^m}{vx^{m-1}}\frac{d\delta_1}{dt}Sc\eta\phi' - \gamma\phi = 0. \tag{12}$$

The transformed boundary conditions are

$$f(0) = 0, f'(0) = \frac{h}{\sqrt{2-\delta}}f''(0), \theta(0) = 1, \phi(0) = 1 \\ f'(\infty) = 1, \theta(\infty) = 0, \phi(\infty) = 0, \tag{13}$$

where $\delta = 2m/m + 1$ is the wedge angle parameter that corresponds to $\Omega = \delta\pi$ for a total angle Ω of the wedge, $M = \sigma B_0^2\delta/\rho$ is the magnetic field parameter, $Pr = \rho C_p v/\lambda_g$ is the Prandtl number, $Nr = \frac{4\sigma^* T_\infty^3}{kK^*}$ is the thermal radiation parameter, $Sc = v/D$ is the Schmidt number, $h = Kn_{x,L}(Re_x)^{1/2}$ is the slip parameter, $Kn = \lambda/x$ is the Knudsen number, $Re_x = Ux/v$ is the Reynolds number, and $\gamma = k\delta^{m+1}/vx^{m-1}$ is the chemical reaction parameter.

Defining $= \frac{\delta^m}{vx^{m-1}}\frac{d\delta}{dt}$, where λ is taken to be a constant, and it can be treated as a dimensionless measure of the unsteadiness, and using λ, Equations (10)–(12) reduce to

$$\left(1 + \frac{1}{\beta}\right)f''' + ff'' + \delta(1 - f'^2) - \lambda(2 - 2f' - \eta f'') - \frac{2}{(m+1)}M(f' - 1)^2 = 0, \tag{14}$$

$$\left(1 + \frac{4}{3}Nr\right)\theta'' + Pr\lambda\eta\theta' + Prf\theta' + \frac{2}{m+1}[A^*e^{-\eta} + B^*\theta] = 0, \tag{15}$$

$$\phi'' + Scf\phi' + \lambda Sc\eta\phi' - \gamma\phi = 0. \tag{16}$$

Further suppose that $\lambda = C/x^{m-1}$, where C is a constant so that $C = \frac{\delta_1^m}{v}\frac{d\delta_1}{dt}$, and, on integrating, it is obtained as

$$\delta_1 = [C(m + 1)vt]^{1/m+1}. \tag{17}$$

When $C = 2$ and $m = 1$ from Equation (17), we obtain $\delta_1 = 2\sqrt{vt}$, which shows that the parameter δ_1 can be compared with the well established scaling parameter [31] for the unsteady boundary layer parameter.

The major physical quantities of interest are the local skin friction, the local Nusselt number, and the local Sherwood number and are defined respectively by

$$C_f Re_x^{\frac{1}{2}}\sqrt{2 - \delta} = 2\left(1 + \frac{1}{\beta}\right)f''(0), \\ Nu \, Re_x^{-\frac{1}{2}}\sqrt{2 - \delta} = -\theta'(0), \\ ShRe_x^{-\frac{1}{2}}\sqrt{2 - \delta} = \phi'(0). \tag{18}$$

3. Results and Discussion

In this paper, the unsteady flow of an incompressible Casson fluid past a wedge under the influence of a transverse magnetic field in conditions of thermal radiation with variable electrical conductivity and velocity wall slip in the presence of a first-order chemical reaction was investigated. The Equations (14)–(16) are coupled nonlinear equations, and it is not possible to get exact analytical solutions. Hence, they can be solved using certain methods like HAM; perturbation techniques; and numerical methods such as the finite difference method, iterative methods, etc. Rashidi and Keimanesh [29] applied the differential transform method and Padé approximant to solve the nonlinear equations of the MHD laminar flow in a liquid film from a horizontal stretching surface. In our analysis, we employed the Runge-Kutta iterative method along with the shooting technique. The numerical work was carried out on an IBM-compatible PC with 4 Gb RAM and a 3.30 Ghz intel core i3 CPU using MATLAB 2008b. The CPU time to obtain the skin friction coefficient,

Nusselt number, and Sherwood number was calculated and is presented in Table 4. To ensure the accuracy of the numerical code, the values $f(0), f'(0),$ and $f''(0)$ are tabulated in Table 1 and compared with the results of White [30] in the absence of $\beta = 0, M = 0,$ and $\lambda = 0$ and are in excellent agreement. The computational results are discussed for several different values of the magnetic field (M), wedge angle (δ), the unsteady parameter (λ), and the Casson parameter (β).

Table 1. Comparison for the Falkner–Skan boundary layer equation for the case of $\lambda = M = Ec = A^* = B^* = \gamma = h = 0, Pr = 0.71, \ Sc = 0.94, \beta \to \infty,$ and $m = 1$

	$f(\eta)$		$f'(\eta)$		$f''(\eta)$	
η	Present work	White [30]	Present work	White [30]	Present work	White [30]
0.0	0.00000	0.0000	0.00000	0.00000	0.469645	0.46960
0.5	0.05864	0.05864	0.23425	0.23423	0.465075	0.46503
1.0	0.23301	0.23299	0.46067	0.46063	0.434418	0.43438
1.5	0.51508	0.51503	0.66153	0.66147	0.361831	0.36180
2.0	0.88687	0.88680	0.81676	0.81669	0.255679	0.25567
3.0	1.79572	1.79557	0.96912	0.96905	0.067705	0.06771
4.0	2.78410	2.78388	0.99783	0.99777	0.006872	0.00687
5.0	3.78352	3.78323	1.00000	0.99994	0.001507	0.00026

Fig. 2 represents the plots of the velocity for different values of wedge angle (δ) (or equivalently, m). Physically, $\delta > 0$ and $m > 0$ correspond to an accelerated flow (i.e., a favorable pressure gradient) and for accelerated flows, the velocity profiles have no point of inflection. For decelerated flow, $m < 0, \ \delta < 0,$ which corresponds to an adverse pressure gradient, the velocity profiles contain a point of inflection. When $m = 0.1103,$ and the wedge angle $\delta = -0.1987,$ flow separation from the wall takes place. White [30] observed flow separation at $\delta = -0.198838.$ The temperature profiles for different values of δ are illustrated in Fig. 3.

The temperature falls steadily throughout the boundary layer and eventually attains its free stream value. For accelerated flow, as δ increases, we observe that the temperature falls. The species concentration profiles for a variation in δ are shown in Fig. 4. It is evident that the species concentration reduces with increasing δ. However, the variation is very minute.

The variation of the Casson parameter on velocity, temperature and concentration is plotted in Figs. 5–7. The velocity profiles indicate that for steady and unsteady flows, the increasing values of the Casson parameter have an increasing influence on the velocity and produce thicker boundary layers. From Fig. 5, it is evident that increasing values of the Casson parameter enhance the rate of transport due to the reduction in the yield stress of the fluid. The velocities are a little higher in the steady case. Fig. 6 reveals that the temperature distribution is observed to decrease throughout the thermal boundary layer with β. This variation is very small as the effect of the Casson parameter does not occur explicitly in the energy equation. The rate of heat transfer decreases with β and the thickness of the associated boundary layers decreases.
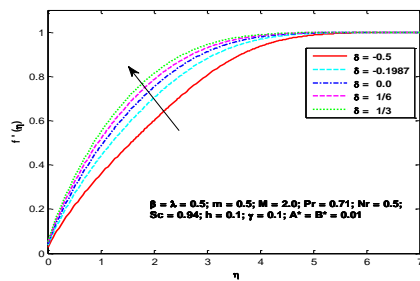

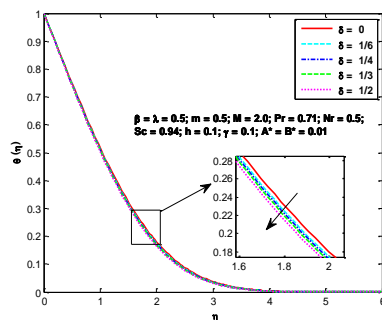
Fig. 2. Velocity profiles for different values of δ
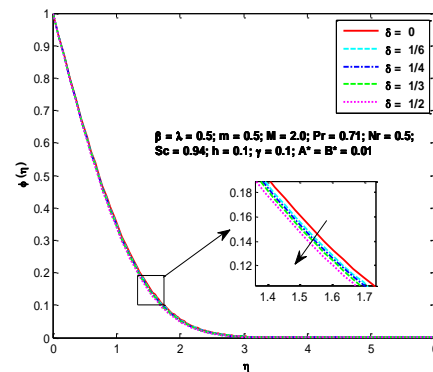

Fig. 3. Temperature profiles for different values of δ

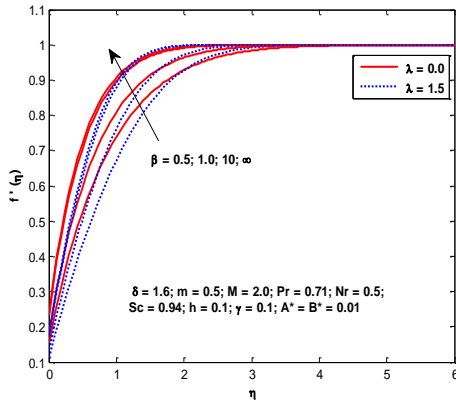Fig. 4. Concentration profiles for different values of δ

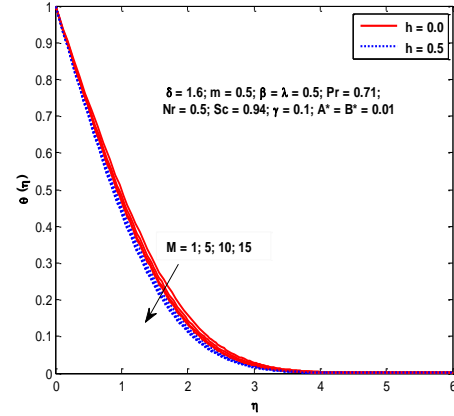Fig. 5. Velocity profiles for different values of β

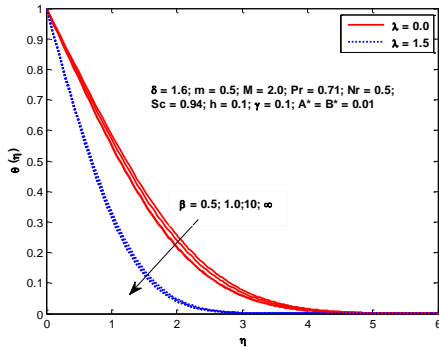Fig. 8. Velocity profiles for different values of M

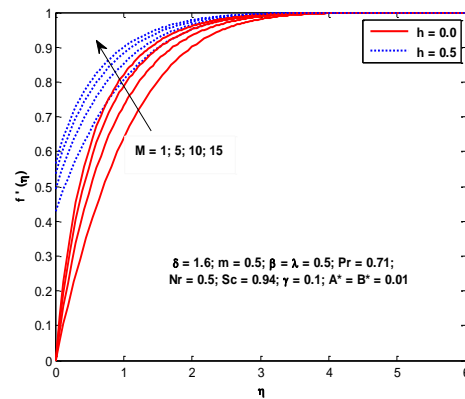Fig. 6. Temperature profiles for different values of β
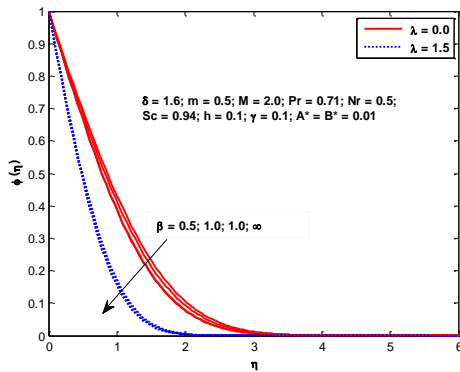

Fig. 9: Temperature profiles for different values of M

Fig. 7. Concentration profiles for different values of β

It was observed that the temperature drops significantly with increasing values of λ, and the associated thermal boundary layers become thinner. From Fig. 7, it can be noticed that an increasing Casson parameter decreases the species concentration at any point. The same trend was noticed by Swati and Mandal [25] in respect to velocity and temperature. The concentration profiles reveal that the rate of mass transfer is enhanced with decreasing values of β, and hence, the thickness of the solutal boundary layer also increases with decreasing β. Further species concentration falls steadily near the boundary and rapidly decreases away from the boundary as λ increases.

The effect of the magnetic field on velocity is illustrated in Fig. 8. It is revealed that the velocity enhances rapidly with an increase in the strength of the magnetic field near the boundary. The application of a magnetic field in an electrical field generates a resistive force viz., the Lorentz force, which generally retards the flow. However, in this case, the applied magnetic field moving with the free stream accelerates the fluid, resulting in the velocity enhancement, and hence, the thickness of the boundary layer increases. Similar behavior was observed by Muhaiman et al. [31, 32].

It was seen that the velocity enhances with an increase in velocity slip (h). The temperature of the fluid is also reduced due to an increase in the magnetic field throughout the thermal boundary layer (Fig. 9). The resulting thermal boundary layers get thinner with increasing M. The temperature was observed to decrease with an increase in the slip parameter. From Fig. 10, it can be concluded that the species concentration also shows a similar trend to that of the temperature for variations in the magnetic field parameter as well as the velocity slip parameter.
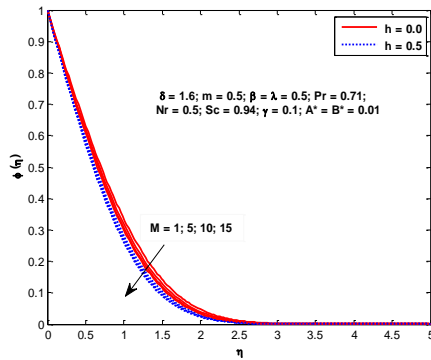
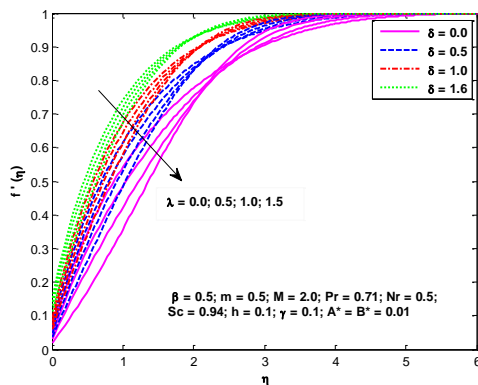Fig. 10. Concentration profiles for different values of *M*
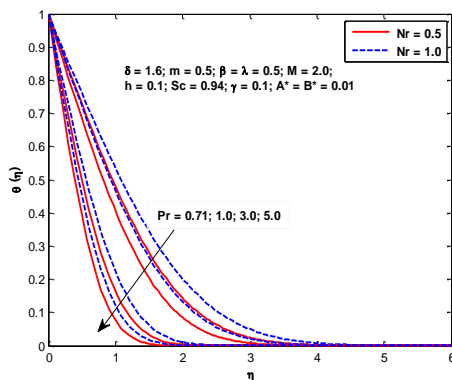

Fig. 11. Velocity profiles for different values of δ and λ

Fig. 12. Temperature profiles for different values of *Pr*

Fig. 11 presents the variation of the unsteady parameter (λ) and wedge angle parameter (δ). For an accelerated flow, it was found that the velocity decreases near the boundar, and is later enhanced, ultimately attaining the free stream value. It also shows the points of flow separation corresponding to the unsteady parameter (λ) for four specific values of the wedge angle parameter (δ). In the case of a horizontal plate ($\delta = 0$), the flow separation occurs at $\lambda = 1.5$; in the case of vertical flat plate, i.e., $\delta = 1/2$, the flow separation occurs at $\lambda = 2$; for stagnation point flow ($\delta = 1$), the flow separation takes place at $\lambda = 2.5$; and in the

case of wedge flow ($\delta = 1.6$), the flow separation is much delayed, i.e., when $\lambda = 3.0$.

Fig. 12 depicts the influence of the Prandtl number and thermal radiation parameter (*Nr*). The temperature was found to reduce with increasing Prandtl number as higher values of the Prandtl number correspond to reducing thermal conductivity. It is evident that the temperature of high–Prandtl number fluids falls more rapidly than low–Prandtl number fluids. The presence of the thermal radiation (*Nr*) increases the temperature significantly throughout the region. The temperature is further increased for the increasing value of *Nr*, and the corresponding thermal boundary layers are thicker. Physically, we may say that there is a pronounced enhancement in the rate of heat transfer from the wedge due to the radiation parameter.

The temperature profiles for different values of the space-dependent and temperature-dependent heat generation/absorption parameters A^* and B^* are plotted in Fig. 13. The temperature has higher values in the presence of a heat source than the values corresponding to the heat absorption case. However, in both cases, as A^* increases, the temperature enhances significantly. The behavior of temperature with the temperature-dependent heat generation/absorption parameter is qualitatively similar to that of A^*.

The species concentration is displayed in Fig. 14 with a varying Schmidt number (Sc) and chemical reaction parameter (γ). It is evident that the species concentration reduces significantly with an increase in the Schmidt number. Higher values of the Schmidt number correspond to lower mass diffusivity, and hence, the solutal boundary layer thickness decreases. Positive values of γ amount to a generative chemical reaction. The species concentration, from its high value on the boundary, steadily decreases throughout the solutal boundary layer, ultimately reaching a value at far infinity. From this figure, it is revealed that there is a pronounced impact on the species concentration as the chemical reaction parameter increases. As the value of the chemical reaction increases, we observed that the species concentration also decreases. The reduction may be due to the fact that the mass transfer increases.
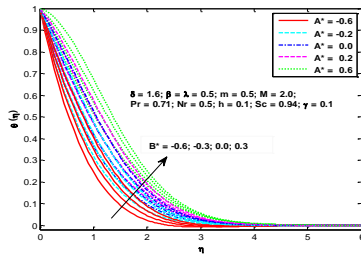
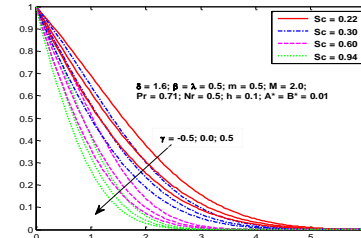Fig. 13. Temperature profiles for different values of A^*

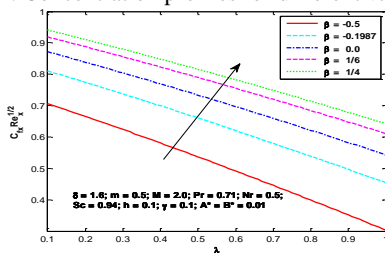Fig. 14. Concentration profiles for different values of Sc

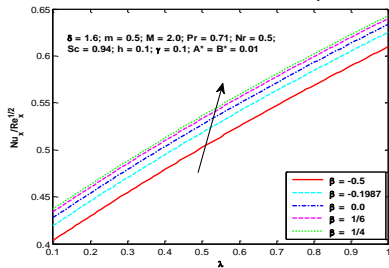Fig. 15. Variation of the skin friction coefficient with λ for different values of β

Fig. 16. Variation of the Nusselt number with λ for different values of β
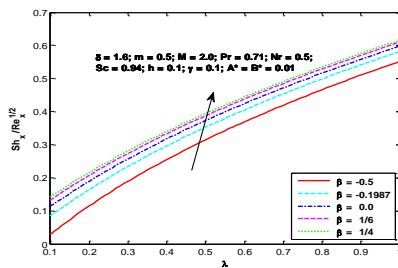

Fig. 17. Variation of the Sherwood number with λ for different values of β

Fig. 15 illustrates the local skin friction coefficient versus the unsteady parameter for different values of the wedge angle parameter. It can be noticed that the skin friction coefficient decreases with an increase in the unsteady parameter. It is also evident that the flow separation occurs for smaller values of δ. The local Nusselt number increases linearly with λ, and it is an increasing function of the wedge angle parameter (Fig. 16). We may conclude that the rate of heat transfer is higher for smaller values of the wedge angle parameter.

The influence of the unsteady parameter increases the local Sherwood number (Fig. 17). When δ is negative, the concentration profiles are not linear, and they become bell-shaped for $\delta = -1.5$.

Table 2 presents the values of $f'(0), -\theta'(0)$ and $\phi'(0)$ for different values of the unsteady parameter λ for variable electrical conductivity (VEC) and constant electrical conductivity (CEC). It can be noticed that in the case of VEC, the values of skin friction, temperature, and concentration gradients on the boundary are higher than in the case of CEC. In both cases of conductivity, the skin friction coefficient decreases for an unsteady flow. With an increase of time, the skin friction is further decreased. In fact, when $\lambda = 0.5$, its value in the case of VEC and CEC is 92.42% and 93% of the value corresponding to that of their steady state values, respectively, and when $\lambda = 2.5$, it is 52.80% and 43.38% of their steady values, respectively. The values of the wall temperature gradient for an unsteady flow were observed to be higher than those of the steady case. Its values at $\lambda = 0.5$ in the case of VEC and CEC are 1.24 and 1.34 times higher than their corresponding steady values, respectively, and when $\lambda = 2.5$ it is double the steady value in the case of VEC and two and half times higher than the steady value in the case of CEC. The concentration gradient on the surface also increases with the unsteady parameter. When $\lambda = 0.5$, the surface concentration gradient is 1.15 and 1.13 times higher than that in the case of VEC and CEC, respectively. When $\lambda = 2.5$ the value for VEC and CEC is 1.63 and 1.86 times the steady state value, respectively.

The local skin friction coefficient reduces linearly with the unsteady parameter. The magnetic field has an enhancing effect on the skin friction coefficient. In addition, the local Nusselt number and Sherwood number linearly increase with the unsteady parameter λ as well as with the magnetic field. The tabulated values of Nusselt numbers indicate that the heat generation/absorption parameter and the radiation parameter increase the rate of heat transfer. It is clear that an increasing Schmidt number, chemical reaction parameter, and Casson parameter enhance the local Sherwood number.

Table 2. Values of $f''(0)$, $-\theta'(0)$, $-\phi'(0)$ for different values of λ in cases of VEC and CEC

λ	$f''(0)$		$-\theta'(0)$		$-\phi'(0)$	
	VEC	CEC	VEC	CEC	VEC	CEC
0.0	1.299060	1.264785	0.407045	0.316289	0.887496	0.757894
0.5	1.200625	1.176254	0.507367	0.426548	1.023139	0.987642
1.0	1.091666	1.063214	0.596071	0.564607	1.145277	1.091961
1.5	0.970741	0.916542	0.674916	0.638900	1.256526	1.193681
2.0	0.836201	0.793645	0.745942	0.739060	1.358940	1.341475
2.5	0.686106	0.54879	0.810759	0.786977	1.454014	1.411638

Table 3. $C_{fx}Re_x^{1/2}$, $Nu_x Re_x^{-1/2}$, and $Sh_x Re_x^{-1/2}$ for various values of pertinent parameters

β	δ	M	m	λ	H	Pr	Nr	A^*	B^*	Sc	γ	$C_{fx}Re_x^{1/2}$	$Nu_x Re_x^{-1/2}$	$Sh_x Re_x^{-1/2}$
0.5	1.6	2.0	0.5	0.5	0.1	0.71	0.5	0.01	0.01	0.94	0.1	0.900803	0.548509	0.812085
1.0												1.067847	0.563244	0.831994
10												1.357420	0.583915	0.861193
∞												1.397750	0.586395	0.864806
0.5	0.0	2.0	0.5	0.5	0.1	0.71	0.5	0.01	0.01	0.94	0.1	0.607058	0.500946	0.749357
	1/6											0.653930	0.507226	0.757012
	1/4											0.675995	0.510116	0.760582
	1/3											0.697189	0.512865	0.764007
0.5	1.6	1.0	0.5	0.5	0.1	0.71	0.5	0.01	0.01	0.94	0.1	0.805454	0.541854	0.802560
		5.0										1.112376	0.561875	0.831429
		10										1.349077	0.574901	0.850572
		15										1.518711	0.583190	0.862919
0.5	1.6	2.0	0.5	0.5	0.1	0.71	0.5	0.01	0.01	0.94	0.1	0.900803	0.546683	0.802560
			1.0									0.855432	0.546891	0.804666
			1.5									0.826068	0.547062	0.807620
			2.0									0.805454	0.547027	0.812085
0.5	1.6	2.0	0.5	0.0	0.1	0.71	0.5	0.01	0.01	0.94	0.1	0.979248	0.417360	0.636292
				0.5								0.900803	0.548509	0.812085
				1.0								0.814804	0.657319	0.960727
				1.5								0.720370	0.751914	1.091164
0.5	1.6	2.0	0.5	0.5	0.0	0.71	0.5	0.01	0.01	0.94	0.1	1.058009	0.527683	0.781472
					0.5							0.568994	0.588353	0.877267
					1.0							0.391186	0.610761	0.912474
					1.5							0.298392	0.622526	0.930916
0.5	1.6	2.0	0.5	0.5	0.1	0.71	0.5	0.01	0.01	0.94	0.1		0.547027	
						1.0							0.641376	
						3.0							1.062233	
						5.0							1.342596	
0.5	1.6	2.0	0.5	0.5	0.1	0.71	0.5	0.01	0.01	0.94	0.1		0.547027	
							1.0						0.481367	
							1.5						0.435861	
							2.0						0.401960	
0.5	1.6	2.0	0.5	0.5	0.1	0.71	0.5	-0.2	0.01	0.94	0.1		0.670592	
								0.0					0.552911	
								0.2					0.435231	
0.5	1.6	2.0	0.5	0.5	0.1	0.71	0.5	0.01	-0.2	0.94	0.1		0.677596	
									0.0				0.553699	
									0.2				0.409122	
0.5	1.6	2.0	0.5	0.5	0.1	0.71	0.5	0.01	0.01	0.22	0.1			0.419246
										0.30				0.482687
										0.60				0.661882
										0.94				0.812085
0.5	1.6	2.0	0.5	0.5	0.1	0.71	0.5	0.01	0.01	0.94	-0.5			0.469665
											0.0			0.761633
											0.5			0.995464

Table 4. CPU time for $C_{fx}Re_x^{1/2}, Nu_x Re_x^{-\frac{1}{2}},$ and $Sh_x Re_x^{-1/2}$

β	δ	M	CPU time		
			$C_{fx}Re_x^{1/2}$	$Nu_x Re_x^{-1/2}$	$Sh_x Re_x^{-1/2}$
0.5 1.0			0.275645	0.307512	0.314375
10	1.6	2.0	0.234375	0.266875	0.278125
∞			0.171875	0.181562	0.205625
			0.156251	0.163293	0.185431
	0		0.304361	0.331875	0.348759
0.5	1/6	2.0	0.245687	0.262546	0.272546
	1/4		0.203125	0.218756	0.224375
	1/3		0.171875	0.183542	0.197953
		1	0.266325	0.279154	0.295672
0.5	1.6	5	0.225321	0.246875	0.255846
		10	0.198756	0.205786	0.219841
		15	0.163458	0.171875	0.173548

4. Conclusion

This analysis presents the effects of non-Newtonian rheology and heat generation/absorption on the unsteady flow of an incompressible Casson fluid over a wedge with slip velocity. From the computational results, it may be inferred that increasing values of the Casson parameter enhances velocity, and temperature and concentration is reduced. The point of flow separation was observed to occur for negative values of δ. The slip parameter enhances the velocity and decreases the temperature and species concentration. The temperature falls with the wedge angle parameter. The radiation parameter and heat generation/absorption enhance the temperature. The Schmidt number, wedge angle, unsteady parameter, and chemical reaction parameter have a reducing influence on the concentration, resulting in thinner solutal boundary layers. The skin friction coefficient is reduced with λ, while it experiences an enhancement with increasing values of δ. The rate of heat transfer decreases with increasing δ. The radiation parameter and heat generation/absorption enhance the rate of heat transfer. The mass transfer rate is reduced with the chemical reaction parameter and Schmidt number. In the case of variable electrical conductivity, the skin friction, temperature, and concentration gradients were found to have higher values than those of the corresponding case of constant electrical conductivity.

Acknowledgements

Nomenclature

B_0 constant

C concentration

c_p specific heat at constant pressure

D mass diffusivity

h slip parameter

k thermal conductivity

k_1 chemical reaction

K^* absorption coefficient

Kn Knudsen number

M Magnetic field parameter

m arbitrary constant

Nr Thermal radiation parameter

Pr Prandtl number

Re_x Reynolds number

Sc Schmidt number

T fluid temperature

u, v velocity components in x and y directions

Greek Symbols

β Casson parameter

σ electrical conductivity

σ^* Stefen-Boltzman constant;

σ_0 constant

δ wedge angle parameter

ν kinematic coefficient of viscosity

ρ density of the fluid

γ chemical reaction parameter

References

[1].Z. Uddin, M. Kumar, S. Harmand, "Influence of thermal radiation and heat generation/absorption on MHD heat transfe flow of a Micropolar fluid past a wedhe with Hall and ion slip currents", Thermal Science, 18, 489–502, (2014).

[2].K. Vajravelu, Swati Mukhopadhya, Fluid flow, heat and mass transfer at bodies of different shapes: Numerical solutions, Academic Press, (2015).

[3].M.M. Rahman, I.A. Eltayeb, "Convective slip flow of rarefied fluids over a wedge with thermal jump and variable transport propertie", International journal of Thermal Sciences, 50, 468–479, (2011).

[4].P.J. Singh, S. Roy, R. Ravindran, "Unsteady mixed convection flow over a vertical wedge", International Journal of Heat and Mass Transfer, 52, 415–421, (2008).

[5].V.M. Falkner, S.W. Skan, "Solutions of the boundary-layer equations", Philosophical Magazine, 7 (12), 865–896, (1931).

[6].D.R. Hartee, "On an equation occurring in Falkner and Skan's approximate treatment of the equations of the boundary layer", Proceedings of the Cambridge Philosophical Society, 33, 223–239, (1937).

[7].K.A. Yih, "MHD Forced Convection Flow Adjacent to a Non – Isothermal Wedge", International Communication Heat Mass Transfer, 26(6), 819–827, (1999).

[8].A.J. Chamka, "MHD Flow of a Uniformly Stretched Vertical Permeable surface in the presence of heat generation/absorption and a chemical reaction", International Communication Heat Mass Transfer, 30, 413–422, (2003).

[9].S.P. Anjali Devi, R. Kandaswamy, "Effects of heat and mass transfer on MHD laminary boundary layer flow over a wedge with suction or injection", Journal of Energy Heat and Mass Transfer, 23, 167–178, (2001).

[10]. R. Kandasamy, B. Abd. Wahid, Md. Raj, A.B. Khamis, "Effects of chemical reaction, heat and mass transfer on boundary layer flow over a porous wedge with heat radiation in the presence of suction or injection", Theoretical Applied Mechanics, 33 (2), 123–148, (2006).

[11]. M. Ganapathirao, R. Ravindran, I. Pop, "Non-uniform slot suction (injection) on an unsteady mixed convection flow over a vertical wedge with chemical reaction and heat generation", International Communication in Heat and Mass transfer, 67, 1054–1061, (2013).

[12]. R. Ahmad, W.A. Khan, "Numerical Study of Heat and Mass Transfer MHD Viscous Flow Over a Moving Wedge in the Presence of Viscous Dissipation and Heat Source/Sink with Convective Boundary Condition", Heat Transfer–Asian Research, 43(1), 17–31, (2014).

[13]. M. Keimanesha, M.M. Rashidi, A.J. Chamkha, R. Jafari, "Study of a third grade non-Newtonian fluid flow between two parallel plates using the multi-step differential transform method", Computers and Mathematics with Applications, 62, 2871–2891, (2011).

[14]. K.R. Rajagopal, A.S. Gupta, T.Y. Na, "A note on the Falkner – Skan flows of a Non –Newtonian fluid", 18(4), 313–320, (1983).

[15]. F.M. Hady, and I.A. Hassanien "Effect of a transverse magnetic field and porosity of the Falkner-Skan flow of a Non – Newtonian fluid", Astrophysics Space Science, 112, 381–391, (1985).

[16]. M.M. Rashidi, M.T. Rastegari, M. Asadi, O. Anwar Beg, "A study of non-Newtonian flow and heat transfer over a non-isothermal wedge using the homotopy analysis method", Chem. Eng. Comm., 199, 231–256, (2012).

[17]. M.S. Alam, S.M.C. Hossain, "A new similarity approach for an unsteady two-dimensional forced convective flow of a micropolar fluid along a wedge", International Journal of Applied Mathematics and Mechanics, 9 (14), 75– 89, (2013).

[18]. B. Rostami, N. M. Rashidi, P. Rostami, E. Momoniat, N. Freidoonimehr, "Analytical Investigation of Laminar Viscoelastic Fluid Flow over a Wedge in the Presence of Buoyancy Force Effects", Article ID 496254, 11, (2014).

[19]. N. Casson, "A flow equation for pigment oil suspensions of printing ink type. In Rheology of Dispersed Systed", (Edited by C.C. Mill), Pergamon Press, Oxford, 84–102, (1959).

[20]. G.V. Vinogradov, A.Y. Malkin, "Rheology of polymers", Mir Publisher, Moscow, (1979).

[21]. W.P. Walwander, T.Y. Chen, D.F. Cala, "An approximate Casson fluid model for tube flow of blood", Biorheology, 12, 111–119, (1975).

[22]. S. E. Charm, G.S. Kurland, "Viscometry of human blood for shear rates of 0-100,000 sec^{-1}", Nature, 206, 617–618, (1965).

[23]. E.W. Merrill, G.A. Pelletier, "Viscosity of human blood: Transition from Newtonian to non-Newtonian", Jour. Appl. Physiol., 33, 178, (1967).

[24].Swati Mukhopadhyay, Iswar Chandra Mondal, Ali J. Chamka, "Casson fluid flow and heat transfer past a symmetric wedge", Wiley Periodical Inc. Heat Transfer Asian Research, 42 (8), 665–675, (2013).

[25]. S. Mukhopadhyay, I.C. Mandal, "Boundary layer flow and heat transfer of a Casson fluid past a symmetric porous wedge with surface heat flux", Chinese Physics B, 23, 1–6, (2014).

[26]. N.T.M. Eldabe, M.G.E. Salwa, "Heat transfer of MHD non – Newtonian Casson fluid flow between two rotating cylinders", J. Phys. Soc. Japan, 64, 41–64, (1995).

[27]. D. Pal, H. Mondal, "MHD non–Darcy mixed convective diffusion of species over a stretching sheet embedded in a porous medium with non–uniform heat source/sink, variable viscosity and Soret effect", Commun Nonlinear Sci Numer Simulat., 17, 672–684, (2012).

[28]. N.G. Kafoussias, N.D. Nanousis, "Magnetohydrodynamic laminar boundary layer flows over a wedge with suction or injection", Can. J. Phys., 75, 733–741, (1997).

[29]. M.M. Rashidi, M. Keimanesh, "Using differential transform method and Pade approximant for solving MHD flow in a lamina liquid film from a horizontal stretching surface", Mathematical Problems in Engineering, 01, 1–14, (2010).

[30]. F.M. White, "Viscous Fluid Flows", Third ed. McGraw-Hill, New York (2006).

[31]. I. Muhaimin, R. Kandasamy, I. Hashim, "Thermophoresis and chemical reaction effects on MHD mixed convective heat and mass transfer past a porous wedge with variable viscosity in the presence of viscous dissipation", International Journal for Computational Methods in Engineering Science and Mechanics, 10, 231–240, (2009a).

[32]. I. Muhaimin, R. Kandasamy, A.B. Kamis, "Thermophoresis and chemical reaction effects on non – Darcy MHD mixed convective heat and mass transfer past a porous wedge in the presence of variable stream function", Chemical Engineering Research and Design, 87, 1527–1535, (2009b).